Unravelling nutrient fate and CO2 concentrations in the reservoirs of the Seine Basin using a modelling approach

Xingcheng Yan, Josette Garnier, Gilles Billen, Shuaitao Wang, Vincent Thieu

Water Research 225 (2022) 119135

Contents lists available at ScienceDirect

Water Research

journal homepage: www.elsevier.com/locate/watres

Unravelling nutrient fate and CO_2 concentrations in the reservoirs of the Seine Basin using a modelling approach

Xingcheng Yan [a,b,*], Josette Garnier [a], Gilles Billen [a], Shuaitao Wang [a], Vincent Thieu [a]

[a] CNRS, EPHE, UMR 7619 METIS, Sorbonne Université, 4 Place Jussieu, Box 105, Paris 75005, France
[b] Center for Eco-Environmental Research, Nanjing Hydraulic Research Institute, Nanjing 210029, China

ARTICLE INFO

Keywords:
Nutrient fate
CO_2 concentration
Modeling approach
Scenario analysis

ABSTRACT

Reservoirs are active reactors for the biogeochemical cycling of carbon (C) and nutrients (nitrogen: N, phosphorus: P, and silica: Si), however, our in-depth understanding of C and nutrient cycling in reservoirs is still limited by the fact that it involves a variety of closely linked and coupled biogeochemical and hydrological processes. In this study, the updated process-based Barman model was applied to three reservoirs of the Seine Basin during 2019–2020, considering the variations of carbon dioxide (CO_2) concentrations and key water quality variables. The model simulations captured well the observed seasonal variations of water quality variables, although discrepancies remained for some variables. According to the model, we found that: (1) the three reservoirs are autotrophic ecosystems and showed high removal efficiency of dissolved inorganic carbon and nutrients during 2019-2020; (2) phytoplankton assimilation, benthic denitrification, precipitation and dissolution of calcium carbonate, and gas exchange at the water-air interface are the dominant processes for water quality variations in reservoirs; (3) based on scenarios results, trophic state and mean water depth of reservoir would impact the biogeochemical processes and the retention efficiency of nitrate and dissolved silicate. Finally, we expect that the successful application of Barman model in the reservoirs of the Seine Basin could provide a useful tool for simulating reservoir water quality changes and thus evaluating the impacts of reservoirs on downstream water quality.

1. Introduction

Inland water ecosystems (river, reservoir, lake, and pond) have been characterized as active sites for carbon (C) and nutrients (e.g., nitrogen: N, phosphorus: P, and silica: Si) biogeochemical cycles (Bastviken et al., 2011; Cole et al., 2007; Deemer et al., 2016; Maavara et al., 2020a; Tranvik et al., 2009; Van Cappellen and Maavara, 2016). Anthropogenic activities may affect nutrient biogeochemical cycles in aquatic ecosystems in several ways, for example, through the increase of nutrient loads to inland waters due to intensive agricultural fertilization and domestic wastewater discharge (Bouwman et al., 2013; Garnier et al., 2021; Grizzetti et al., 2021), and through disturbances along the aquatic continuum (Friedl and Wüest, 2002; Maavara et al., 2020a; Van Cappellen and Maavara, 2016). The construction of reservoirs represents a significant human disturbance to the integrity of inland water ecosystems, and its impact on the C and nutrient biogeochemical cycles has led to substantial interest in reservoir biogeochemical research in recent years (Chen et al., 2020; Deemer et al., 2016; Harrison et al., 2021; Maavara et al., 2020b, 2020a; Wang et al., 2018, 2021; Yan et al., 2021a).

Reservoirs are usually built by damming a river, significantly altering hydrological conditions, transforming a lotic ecosystem into a lentic ecosystem (Schmutz and Moog, 2018), impeding the natural flow of water and the associated C and nutrients, and acting as the in-stream reactors (Maavara et al., 2020a). Typically, reservoirs increase the water residence time and sedimentation rate, and thus decrease turbidity and light attenuation in the reservoir water column, providing favorable conditions for promoting photosynthesis and enhancing C and nutrient biogeochemical cycling (Van Cappellen and Maavara, 2016). Photosynthesis assimilates dissolved inorganic carbon (DIC) and nutrients into organic matter, which is further decomposed by several processes (e.g., aerobic respiration, denitrification, dissolution of biogenic silica), and thereby impacts the concentrations of carbon dioxide (CO_2) and nutrients in the water column (Li et al., 2022; Wang et al., 2020a, 2020b; Xiao et al., 2021). Therefore, the variations of CO_2 and nutrient concentrations in reservoirs are indeed closely linked through multiple

* Corresponding author at: CNRS, EPHE, UMR 7619 METIS, Sorbonne Université, 4 Place Jussieu, Box 105, Paris 75005, France.
E-mail address: xingcheng.yan@upmc.fr (X. Yan).

https://doi.org/10.1016/j.watres.2022.119135
Received 18 May 2022; Received in revised form 16 September 2022; Accepted 16 September 2022
Available online 18 September 2022

biogeochemical processes. However, these processes remain difficult to understand through *in situ* measurements (Kong et al., 2019).

Process-based biogeochemical models have been well developed to simulate the water quality variables (e.g., water temperature and nutrient budgets) in inland aquatic ecosystems (Mooij et al., 2010). There are a number of well-established aquatic ecosystem models simulating water quality that have been applied to reservoirs including the CE-QUAL-W2 (e.g., Lindenschmidt et al., 2019; Sadeghian et al., 2018; Wu et al., 2022), EFDC (e.g., Tong et al., 2021), and Delft3D models (e.g., Chen et al., 2019). In addition, some other models were specifically designed for stagnant systems and for simulating the dynamics of water quality variables in reservoirs, such as the PCLake (Kong et al., 2019), Barman (Garnier et al., 2000; Thieu et al., 2006), DyLEM-1D (Bonnet and Poulin, 2004) and GLM model (Weber et al., 2017; Winton et al., 2021). To the best of our knowledge, few studies have assessed both nutrient fate and CO_2 concentrations in reservoirs using process-based biogeochemical models. As mentioned previously, the variations of CO_2 and nutrient concentrations are co-impacted by the biogeochemical processes occurring in the reservoirs; therefore, we argue that models that take into account both nutrient fate and CO_2 variations could provide new insights into the biogeochemical functioning of reservoirs.

To address the aforementioned question, we focused on investigating the applicability of an existing process-based biogeochemical model in the main reservoirs of the Seine Basin (France). The nutrient budgets in these reservoirs have been explored by *in situ* measurements, mass balance methods (Garnier et al., 1999; Yan et al., 2022, 2021b), and an initial modeling approach (Garnier et al., 2000; Thieu et al., 2006). Here, we applied the Barman model, which newly contains an inorganic carbon module based on a previous study on the Seine River (Marescaux et al., 2020). The specific goals of the present study are as follows: (1) to evaluate the performance of the Barman model in simulating the variations of nutrient and CO_2 concentrations in the reservoirs; (2) to quantify the nutrient fate and related biogeochemical processes; (3) to discuss the impact of potential scenarios, including trophic states, hydrological management strategies, and morphological characteristics, on the ecological functions of these reservoirs; and (4) to propose science-based options and implications for the downstream targeted nutrient management in reservoirs.

2. Material and methods

2.1. The Marne, Aube, and Seine reservoirs

The three main reservoirs (Marne, Aube, and Seine) are located upstream of the Seine Basin, with a maximum surface area of 48 km^2, 23 km^2, and 23 km^2, respectively (Fig. 1); they are managed by the public institution *Seine Grand Lac* (SGL, https://www.seinegrandslacs.fr/).

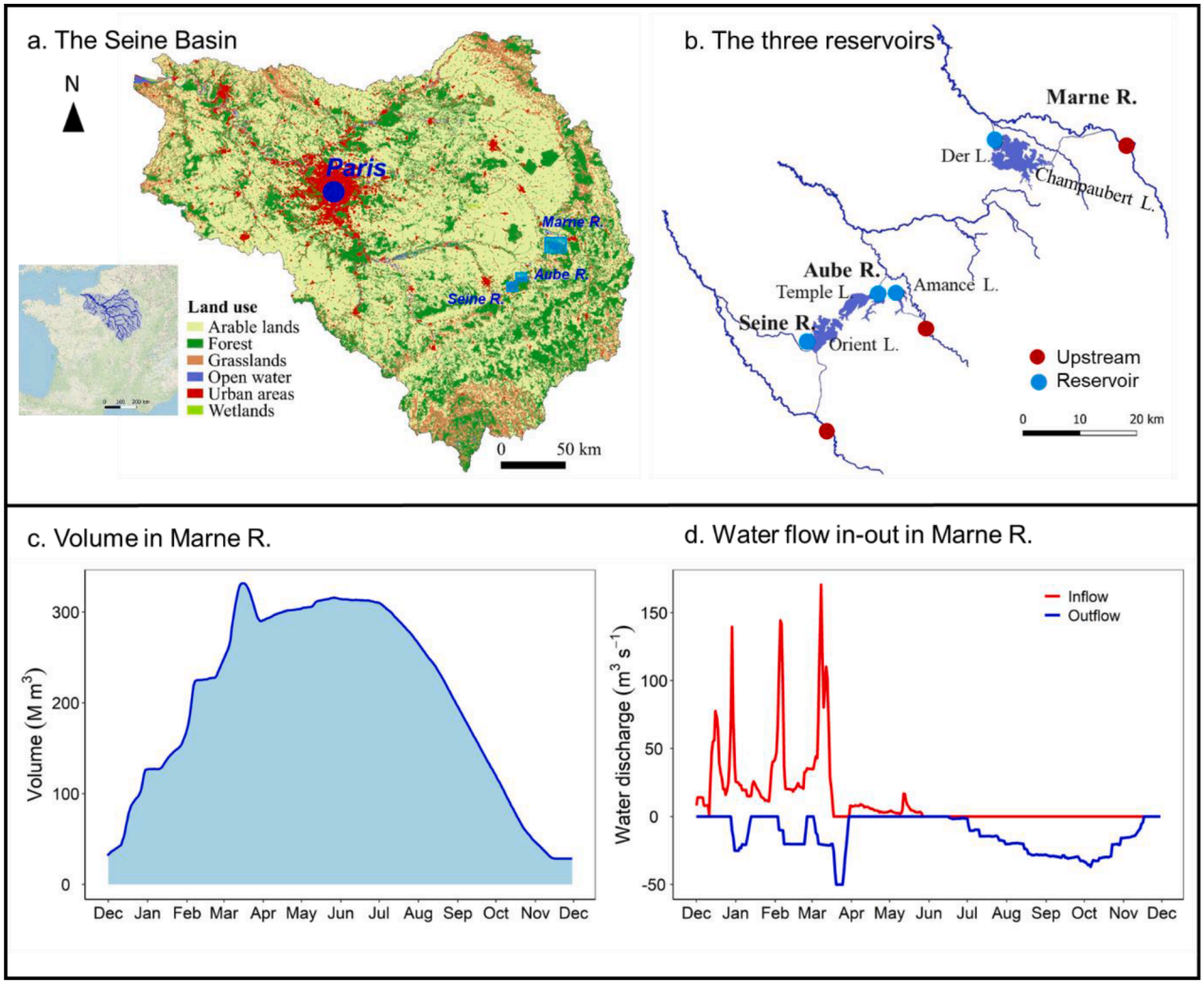

Fig. 1. a. The Seine Basin and its location in France. b. Diagram of the three diverted reservoirs in the Seine Basin. The blue and red dots indicate the sampled sites in the three reservoirs and their upstream rivers, respectively. The Marne Reservoir was taken as an example to present the typical annual hydrological characteristics of the three reservoirs from December 2019 to November 2020, including (c) the reservoir's volume variation and (d) water discharge, flowing in-out.

Table 1
Main characteristics in the three studied diverted reservoirs*.

Reservoir	Marne	Aube_Amance	Aube_Temple	Seine
Maximum surface area (km^2)	48	7	17	23
Volume (Mm^3, range)	27–330	13–22	19–140	16–199
Mean depth at maximum level (m)	7.2	3.5	7.6	8.9
Lithology	Clay			
Agriculture land	38.47%	38.25%		48.24%
Grassland	17.92%	6.29%		4.81%
Forest	39.90%	53.72%		45.26%
Inflow discharge ($m^3\ s^{-1}$, range)	0–150	0–40		0–62
Outflow discharge ($m^3\ s^{-1}$, range)	0–50	0–15		0–25
Discharge of upstream river ($m^3\ s^{-1}$, range)	2–256	1–123		2–127
pH	7.9–8.7	8.0–8.7	7.9–8.7	7.8–8.5
T (°C, range)	5.1–24.2	6.8–24.8	6.8–24.8	7.6–24.6
DO (mg $O_2\ L^{-1}$, range)	8.3–12.0	8.6–13.6	8.3–11.8	6.6–12.8
Chl–*a* (μg L^{-1}, range)	2.0–38.8	1.0–11.6	1.8–20.9	1.5–71.3
NO_3^- (mg N L^{-1}, range)	0.2–5.5	0.2–4.6	0.3–4.3	0.7–6.3
PO_4^{3-} (mg P L^{-1}, range)	0–0.08	0–0.05	0–0.04	0–0.02
DSi (mg Si L^{-1}, range)	0.07–2.0	0.12–2.3	0–2.0	0.03–2.1

* Annual hydrological data was used to present the hydrological characteristics of these reservoirs; variations of water quality variables were provided based on field campaigns during April 2019 and November 2020 (Values from surface waters for water quality variables).

These reservoirs are diverted from their upstream rivers and linked to downstream rivers through artificial canals. The Aube Reservoir contains two distinct lakes, Lake Amance and Lake Temple. The two main hydrological functions of these reservoirs are to prevent downstream flooding during winter and spring, and to support downstream low water flow in summer and autumn. Therefore, the annual hydrological cycle (from December 2019 to November 2020) of these three reservoirs is similar (see Fig. 1c and d) and can be characterized by two periods: the filling period (water flows into the reservoirs, from December to June of the following year) and the emptying period (water flows out of the reservoirs, from July to November). The main characteristics of the three reservoirs were presented in Table 1.

2.2. Data collected on the field

The water quality in the three reservoirs and their upstream rivers was acquired through monthly field measurements during 2019 and 2020. The sampling strategy for each site (see Yan et al., 2022) was to take water with a bucket from bridges or pontoons; 5–L high-density polyethylene sampling bottles were filled. All samples were conditioned (e.g., filtration) and kept at < 10 °C in the field. After returning to the laboratory, they were stored at 4 °C or frozen until the analysis.

In the field, pH, water temperature (T,°C), and dissolved oxygen (DO, mg L^{-1}) were measured using a multiparameter instrument (YSI ® 6600 V2). For CO_2 measurements, 30 mL of water was kept in four syringes (60 mL) with 30 mL of ambient air, and were shaken for 10 min. A fifth syringe was filled with ambient air to measure the atmospheric CO_2. The partial pressure of CO_2 (pCO_2) in water was determined through a non-dispersive infrared gas analyzer (Licor, LI–820, USA) using the syringe headspace equilibrium method (Abril et al., 2015; Marescaux et al., 2018).

In the laboratory, dissolved nutrient concentrations, including nitrate (NO_3^-, mg N L^{-1}), nitrite (NO_2^-, mg N L^{-1}), ammonium (NH_4^+, mg N L^{-1}), orthophosphate (PO_4^{3-}, mg P L^{-1}), and dissolved silicate (DSi, mg Si L^{-1}) were measured spectrophotometrically according to Slawyk and MacIsaac (1972), Rodier (1984), and Jones (1984), respectively. Suspended particulate matters (SM, mg L^{-1}) were determined as the weight of material retained on a Whatman GF/F membrane per volume unit after drying the filter for 2 h at 120°C. The total inorganic phosphorus (TIP, mg P L^{-1}) was calculated by PO_4^{3-} and SM according to Billen et al. (2007) and Némery et al. (2005). For the analysis of dissolved organic carbon (DOC, mg C L^{-1}), water samples were filtered with GF/F Whatman grilled filters (GF/F, 0.7 μm, at 500°C for 4 h), collected in grilled glass flasks and acidified (0.1 mL H_2SO_4, 4 M in 30 mL of water), and then analyzed with a TOC analyzer (Aurora 1030 TOC Analyzer, OI Analytical). Chlorophyll a concentrations (Chl-*a*, μg L^{-1}, algal cells retained on GF/C membrane filters) were determined spectrophotometrically after extraction using 90% acetone according to Lorenzen (1967). TA (mmol L-1) was measured by 20 mL of filtered water (GF/F: 0.7 μm) using an automatic titrator (Titrando 905) and HCl (hydrochloric acid, 0.01 M). DIC (mg C L^{-1}) concentrations were calculated from water temperature, pH, and TA using CO_2SYS (Pierrot et al., 2006).

2.3. The Barman model

The Barman model was applied to the Marne Reservoir during 1993–1995 with a simplified representation of the hydraulic conditions of the reservoir, considered as a perfectly mixed biogeochemical reactor (Garnier et al., 2000) and coupled with a detailed process-based biogeochemical model (the RIVE model, Billen et al., 1994; Garnier et al., 2002). Additional developments have introduced a simplified representation of the reservoir's morphology (as idealized parabolic or spherical shapes), and the possibility to simulate the average depth of the reservoir according to the management of the water volumes at each time step (Thieu et al., 2006). Recently recoded in Python, both the RIVE (v3.2, https://gitlab.in2p3.fr/rive/pyrive) and Barman (https://gitlab.in2p3.fr/rive/barman) models have been published under the terms of the EPL-2.0 Eclipse Public License and the GNU GPL-3.0 General Public License. The current version of the Barman model has embedded the latest version of the RIVE code (pyRive, v3.2), including the calculations of the biogeochemical processes and nutrient exchanges at the water–sediment interface by a simplified algorithm method (Billen et al., 2015), and the inorganic carbon module was implemented to simulate CO_2 concentrations in rivers (Marescaux et al., 2020). Detailed descriptions of the Barman, including morphological characteristics (Table S1 and Fig. S1), and the RIVE models are presented in the supplementary information (SI, Text S1 and Fig. S2). The parameters used in the RIVE model are shown in Table S2.

Additionally, we updated the calculations of total alkalinity (TA) and DIC based on Marescaux et al. (2020). In these reservoirs, we found that precipitation and dissolution of calcium carbonate ($CaCO_3$) are significant (see Text S2, Fig. S3); therefore, we considered the effect of $CaCO_3$ precipitation and dissolution on changes in TA and DIC. The equations for calculating TA and DIC are as follows:

$$TA = TA_{t-1} + d_t \frac{dTA}{d_t} \quad (1)$$

$$\frac{dTA}{d_t} = \left[\left(\frac{14}{106} \times \frac{(respBact + respZoo + respBent)}{12}\right) + \frac{(denit - 2{\cdot}nitr[AOB^{'}])}{14} + \left(\frac{17}{106} \times \frac{uptPhyNO_3^-}{uptPhyN} - \frac{15}{106}\frac{uptPhyNH_4^+}{uptPhyN}\right) \times \frac{uptPhyC}{12} - \left(\frac{CaPrecip}{40} \times 2\right)\right] \times 1000 - dilu\left(TA_{t-1} - TA_{input}\right) \quad (2)$$

$$DIC = DIC_{t-1} + d_t \frac{dDIC}{d_t} \quad (3)$$

$$\frac{dDIC}{d_t} = (respBact + respZoo + respBent) + \frac{\text{denit}}{14} \times 12 \times \frac{5}{4} - uptPhyC + \frac{F_{CO_2}}{depth} - \frac{CaPrecip}{40} \times 12 - dilu\left(DIC_{t-1} - DIC_{input}\right) \quad (4)$$

where TA_{t-1} and DIC_{t-1} are the values of TA and DIC in the previous time step (t−1), and TA_{input} (μmol L^{-1}) and DIC_{input} (mg C L^{-1}) are the TA and DIC inputs from upstream rivers, respectively. In the RIVE model, respBact, respZoo, and respBent represent the respiration of bacteria, zooplankton, and benthic respiration (mg C L^{-1} h^{-1}), respectively; denit and nitr['AOB'] are, respectively, the denitrification and nitrification (by ammonia-oxidizing bacteria [AOB], mg N L^{-1} h^{-1}); uptPhyN is the nitrogen uptake by phytoplankton (mg N L^{-1} h^{-1}), consisting of nitrate ($uptPhyNO_3^-$, mg N L^{-1} h^{-1}) and ammonium ($uptPhyNH_4^+$, mg N L^{-1} h^{-1}); uptPhyC is the inorganic carbon uptake by phytoplankton (mg C L^{-1} h^{-1}); F_{CO_2} (mg C m^{-2} h^{-1}) is the CO_2 flux at the water–air interface (refer to Yan et al., 2022); *depth* is the mean water depth of the reservoir (m); dilu represents the mixing effect caused by water entering the reservoir (h^{-1}); CaPrecip is the $CaCO_3$ precipitation/dissolution rate, which was reflected by the obvious seasonal dynamics of Ca^{2+} concentrations in the three reservoirs (see Text S2).

Once TA and DIC are calculated, the hydrogen ion concentration (H^+) can be calculated based on TA and DIC, and CO_2 can be derived from H^+ and TA/DIC (Stumm and Morgan, 1996). The calculation procedures of H^+ and CO_2 are presented in Text S3.

2.4. Model implementation and evaluation

The quantity and quality of water flowing into the reservoir are the main boundary conditions of the Barman model. The daily dynamics of volume and mean depth of the reservoir were calculated according to the idealized morphology and the water discharge flowing into and out of the reservoir, provided by the SGL. The water quality variables used are those collected on the field (see Section 2.2).

Interpolation methods were applied to derive the input data at the daily time step. The WRTDS (weighted regressions on time, discharge, and season) method was used for water quality variables, including NO_3^-, DSi, SM, and PO_4^{3-} (e.g., Hirsch et al., 2010; Zhang and Blomquist, 2018), which are presented in Fig. S4. A simple linear interpolation method was used for other water variables.

The RMSE (root mean square error) and bias were used to evaluate the performance of the Barman model:

$$\text{RMSE} = \sqrt{\sum_{i=1}^{n} (obs_i - sim_i)^2 / n} \quad (5)$$

$$\text{Bias} = \sum_{i=1}^{n} (obs_i - sim_i) / \sum_{i=1}^{n} obs_i \quad (6)$$

where *n* is the number of observations and obs and sim are the observed and simulated concentrations, respectively.

2.5. Scenario setup

In order to deepen our understanding of the factors influencing reservoir biogeochemical processes and functions, an analysis of three possible scenarios were conducted using the Marne Reservoir as an example, including (1) trophic state: different TIP concentration in the incoming river flow; (2) hydrological management alterations: delaying and advancing the emptying period for one month; (3) morphological characteristic: theoretical reservoir shape was created on the basis of the initial calibration of the reservoir morphology (Text S1) and using maximum depth (D_{max}) and surface area (S_{max}) parameters to estimate the daily variation in the mean depth and volume of the Marne Reservoir. The detailed scenario setup is presented in Table 2.

Table 2
Details of scenario setup and analysis in Marne Reservoir, as an example.

Scenarios	Setup	Analysis
Trophic state	**Different TIP concentrations in upstream river** **Ref.:** ~ 20 μg P L^{-1} **TIP gradients:** 1, 5, 10, 12, 15, 20, 25, 50, 100 μg P L^{-1}	The impact of each scenario on the ecosystem metabolism (primary production and respiration) and on nutrient retentions (NO_3^- and DSi) were explored. For each scenario analysis, no change was made to other boundary conditions and morphological changes preserved the initial semi–spherical shape and the maximum volume capacity of reservoir (see Text S1).
Hydrological management alteration	**Different emptying period** **Ref.**: from July to November **Advance:** from June to November **Delay:** from August to November	
Morphological characteristics	**Different maximum depth (D_{max}) and surface area (S_{max})** **Ref.:** D_{max} = 17.28 m, S_{max} = 49.78 km^2 **High D_{max} and small S_{max}** (small and deep reservoir): D_{max} = 25 m, S_{max} = 33 km^2 **Low D_{max} and large S_{max}** (large and shallow reservoir): D_{max} = 9 m, S_{max} = 100 km^2	

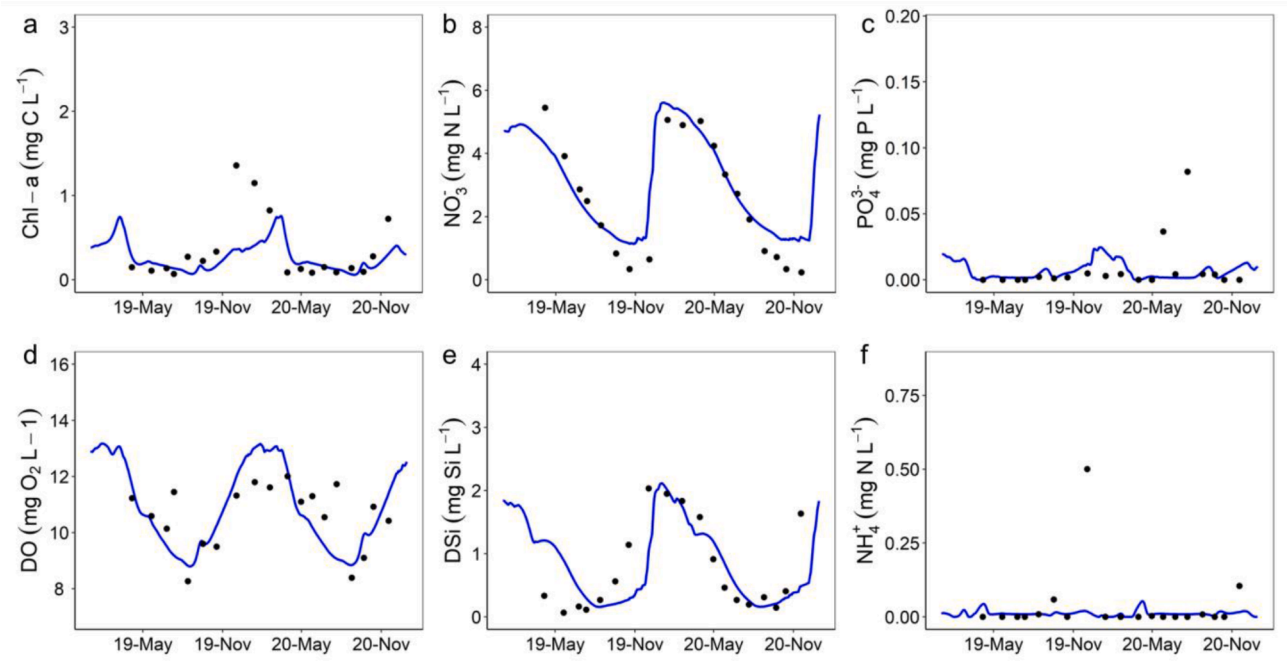

Fig. 2. Simulations and observations of the water variables in the Marne Reservoir (2019–2020). (a) Chl-*a*, (b) NO_3^-, (c) PO_4^{3-}, (d) DO, (e) DSi, (f) NH_4^+. The blue line represents the simulation results, and the black dots are the observations.

Table 3
Root mean square error (RMSE) and bias for chlorophyll *a* (Chl–*a*, mg C L^{-1}), nitrate (NO_3^-, mg N L^{-1}), orthophosphate (PO_4^{3-}, mg P L^{-1}), dissolved oxygen (DO, mg O_2 L^{-1}), dissolved silicate (DSi, mg Si L^{-1}), ammonium (NH_4^+, mg N L^{-1}), total alkalinity (TA, μmol L^{-1}), pH (–), dissolved inorganic carbon (DIC, mg C L^{-1}), and carbon dioxide (CO_2, mg C L^{-1}). *n* = number of data for the calculations.

Reservoirs		*n*	Chl–*a*	NO_3^-	PO_4^{3-}	DO	DSi	NH_4^+	TA	pH	DIC	CO_2
Marne R.	RMSE	19	0.50	0.76	0.02	1.09	0.52	0.11	348.69	0.28	4.13	0.24
	Bias	19	0.03	–0.10	0.34	0.01	0.06	0.63	–0.03	0.003	–0.03	–0.15
Seine R.	RMSE	18	0.66	0.63	0.01	1.78	0.48	0.23	486.09	0.31	5.63	0.43
	Bias	18	0.03	0.07	–0.47	0.06	–0.63	0.79	–0.09	–0.01	–0.09	0.03
Aube R. Amance	RMSE	13	0.18	0.8	0.01	1.29	0.46	0.03	891.3	0.48	10.28	0.25
	Bias	13	0.03	–0.12	0.37	0.02	0.38	0.37	–0.23	–0.03	–0.21	–0.18
Aube R. Temple	RMSE	19	0.30	0.66	0.01	0.72	0.56	0.03	901.10	0.28	10.78	0.22
	Bias	19	0.03	0.07	0.13	0.0002	–0.18	0.25	0.31	0.01	0.31	–0.28

3. Results

3.1. Model performance

3.1.1. Validation of the dynamics in water quality variables

Because the dynamics of the water quality variables were similar in the three reservoirs, we present here the Marne Reservoir as an example (Fig. 2) and the results of the other two reservoirs are presented in SI (Figs. S5–S7). Overall, despite some discrepancies between observations and simulations, the simulation well results reproduce the observations of key water variables in the three reservoirs during 2019–2020. The RMSE and bias, which indicate the deviation and the over-/underestimations between observations and simulations in the three reservoirs, respectively, show values well in the range, except for the high values of PO_4^{3-} and NH_4^+ concentrations (Table 3). The model successfully simulated phytoplankton development (Fig. 2a) during December–March and April–August, respectively; however, the model led to a lag in simulating the gradual increase of Chl-*a* during September–December and did not capture the peak value of Chl-*a* in December. The model showed a good simulation of NO_3^- dynamics during December–July, but it slightly overestimated the low NO_3^- concentrations during September–November (at the end of the emptying period). For DO, the model successfully captured the general trend in the reservoirs, with high and low values during December–March and August–September, respectively. Moreover, the seasonal variations of DSi concentrations in the three reservoirs were successfully simulated by the model during 2019–2020, including the gradual decrease during December–August (of the following year) and the increase during September–November (Fig. 2). In addition, the model also captured most observations of PO_4^{3-} and NH_4^+, except for some high values (e.g., PO_4^{3-} in May and July of 2020, and NH_4^+ in November of 2019 and 2020 in the Marne Reservoir).

3.1.2. Validation of the CO_2 simulation

In the carbonate systems, the model successfully simulated the dynamics of TA and DIC in the three reservoirs during 2019–2020 (Figs. 3 and S5-S7). In addition, we also found that the precipitation and dissolution of $CaCO_3$ play a significant role in regulating the dynamics of TA and DIC in the three reservoirs compared with the effect of the biogeochemical processes (Text S4 and Fig. S8). Although the observed values of pH in the reservoirs fluctuated, the model still captured the general level of pH; however, discrepancies between simulations and observations still exist during March–July 2020, not adhering well to the trend and with some underestimations of the pH. Nevertheless, the simulations of CO_2 were generally consistent with the observations, i.e., the relatively high and low values, and the decrease in CO_2 was captured.

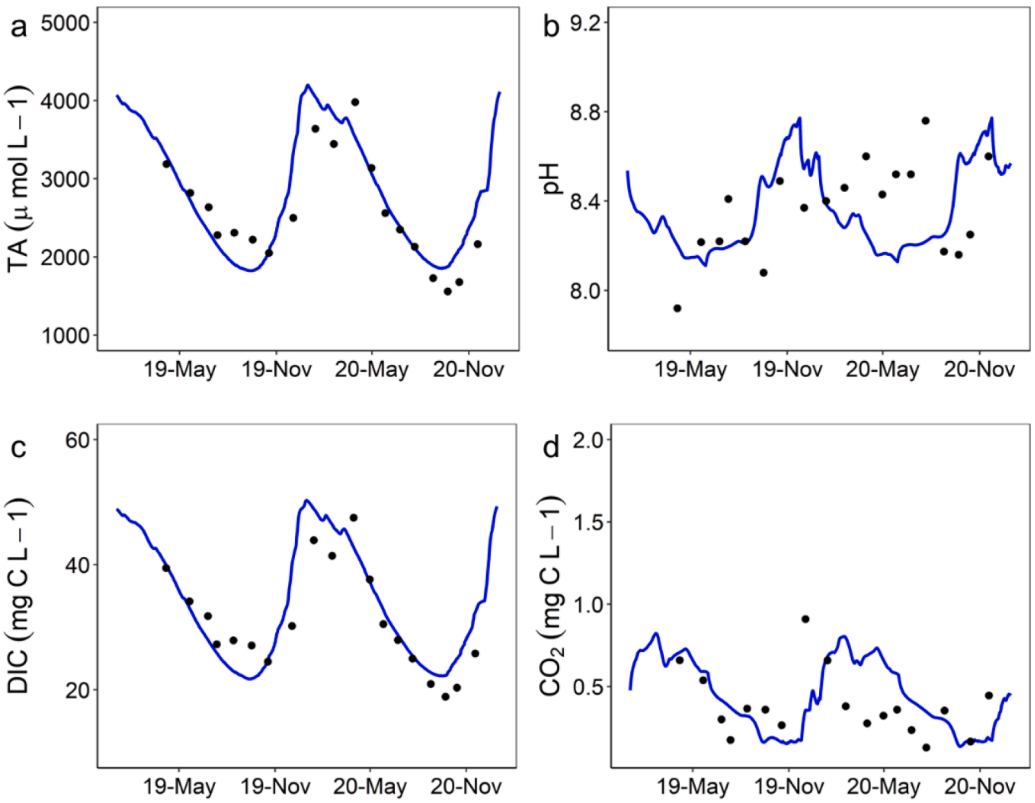

Fig. 3. Simulations and observations of the CO_2 systems in the Marne Reservoir (2019–2020). (a) TA, (b) pH, (c) DIC, and (d) CO_2. The blue line represents the simulation results, and the black dots are the observations.

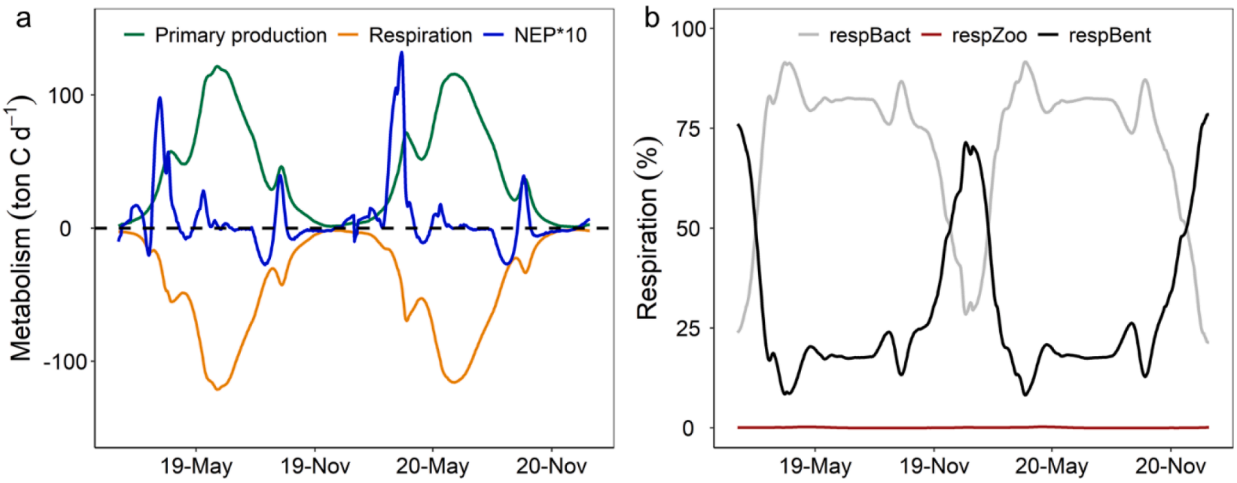

Fig. 4. Daily ecosystem metabolism in the Marne Reservoir from 2019 to 2020, including (a) primary production (phytoplankton uptake), respiration, and NEP (net ecosystem production = photosynthesis − respiration), the black dashed line indicates the balanced metabolism (primary production equal to respiration); (b) the contribution of bacterial respiration (respBact), zooplankton respiration (respZoo), and benthic respiration (respBent) to total respiration.

3.2. The biogeochemical processes and nutrient fate in the three reservoirs

3.2.1. The ecosystem metabolism

Primary production and respiration rates showed synchronized variations in the three reservoirs, gradually increasing from January to July, while decreasing from July to December (Fig. 4 for the Marne Reservoir; the others refer to Fig. S9). The highest rates of primary production (i.e., phytoplankton uptake) were found during June–July, from 23 tons C d^{-1} in Aube–Amance to 115 tons C d^{-1} in Marne, which is the largest reservoir with twice the surface area of the former reservoirs. The highest respiration rates were very close to the phytoplankton uptake rates. In terms of net ecosystem primary production (NEP, i.e., photosynthesis minus respiration), the three reservoirs were generally autotrophic ecosystems, with average NEP values from 0.16 to 0.79 tons C d^{-1} (ranging from 57 [Aube–Temple] to 288 [Marne] tons C yr^{-1} during one annual hydrological cycle). In the model, respiration represents the sum of bacteria (respBact), zooplankton (respZoo), and benthic respiration (respBent). The results revealed that respBact and respBent were the dominant components of total respiration, while respZoo made only a small contribution to this total in the three reservoirs. Indeed, respBact represented more than 75% of the total respiration during March–October, which corresponded to the period with high primary

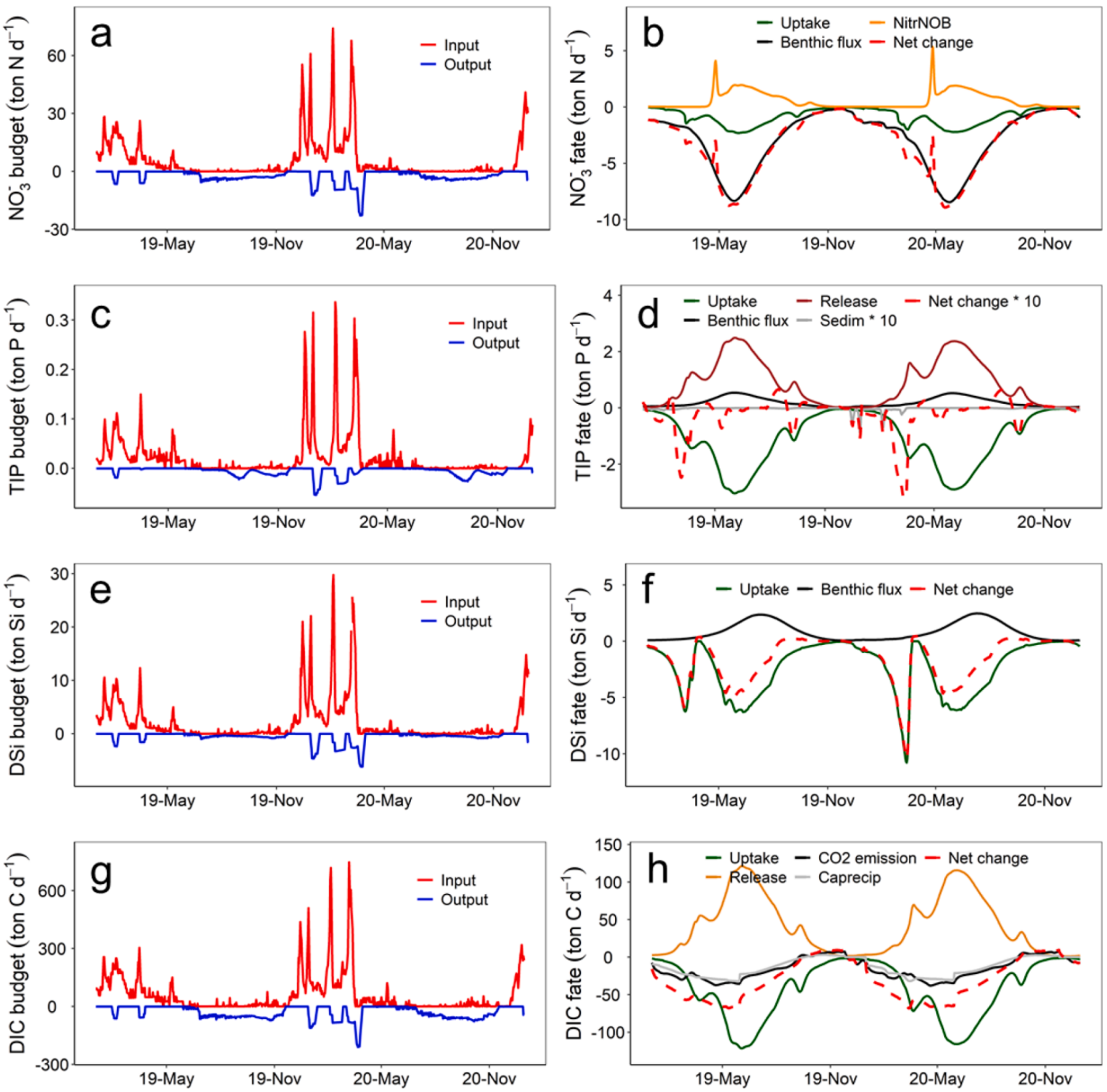

Fig. 5. Budgets of NO_3^- (a), TIP (c), DSi (e), and DIC (g) based on interpolated upstream concentrations (input fluxes, red lines) and the Barman model simulation (output fluxes, blue lines). Associated simulated biogeochemical processes, with positive and negative values indicating respectively an increase or decrease of NO_3^-(b, NitrNOB is nitrite oxidation in the water column), TIP(d), DSi (f) and DIC (h) concentrations in the water column, respectively. The dashed red line represents the net change of nutrient concentrations in the water column.

production, and a high respBent rate was found during November–February (of the following hydrological year) in the three reservoirs.

3.2.2. *Nutrient fate and corresponding biogeochemical processes*

The input and output fluxes of NO_3^-, TIP, DSi, and DIC and the main biogeochemical processes related to their transformations were quantified during 2019 and 2020 (Fig. 5 for Marne; for the others, refer to Figs. S10–12). In terms of the fate of nutrients, the results revealed that phytoplankton uptake was one of the most significant processes affecting the transformations of NO_3^-, TIP, DSi, and DIC in the three reservoirs. Benthic denitrification, especially, and nitrification in the water column were also two important processes affecting NO_3^- dynamics in the three reservoirs. Internal cycling of P was enhanced by phytoplankton uptake, respiration, and benthic release, while the sedimentation of TIP had a marginal impact on TIP in the water column compared with the other processes. For DSi, diatom uptake played an important role in DSi concentrations in the water column, and benthic flux released by biogenic silica dissolution (BSi) did not compensate for this. In terms of the DIC transformation, phytoplankton uptake and respiration were two dominant processes regulating the internal cycling of DIC, while the precipitation of $CaCO_3$ and CO_2 emissions was the dominant process driving the net change of DIC concentrations in the water column.

3.2.3. *Nutrient budgets during one hydrological cycle*

In the three reservoirs, the N budgets (including NO_3^- and NH_4^+), P (TIP), Si (DSi and BSi), and C (including total organic carbon and inorganic carbon) during one annual hydrological cycle were calculated according to the multiple processes considered by the Barman model. Here, we show schematic diagrams of nutrient transformation and transport in the example of the Marne Reservoir (Fig. 6); details on the nutrient fate of the three reservoirs are provided in Table S3. All three reservoirs affected a high NO_3^- retention, ranging from 36%

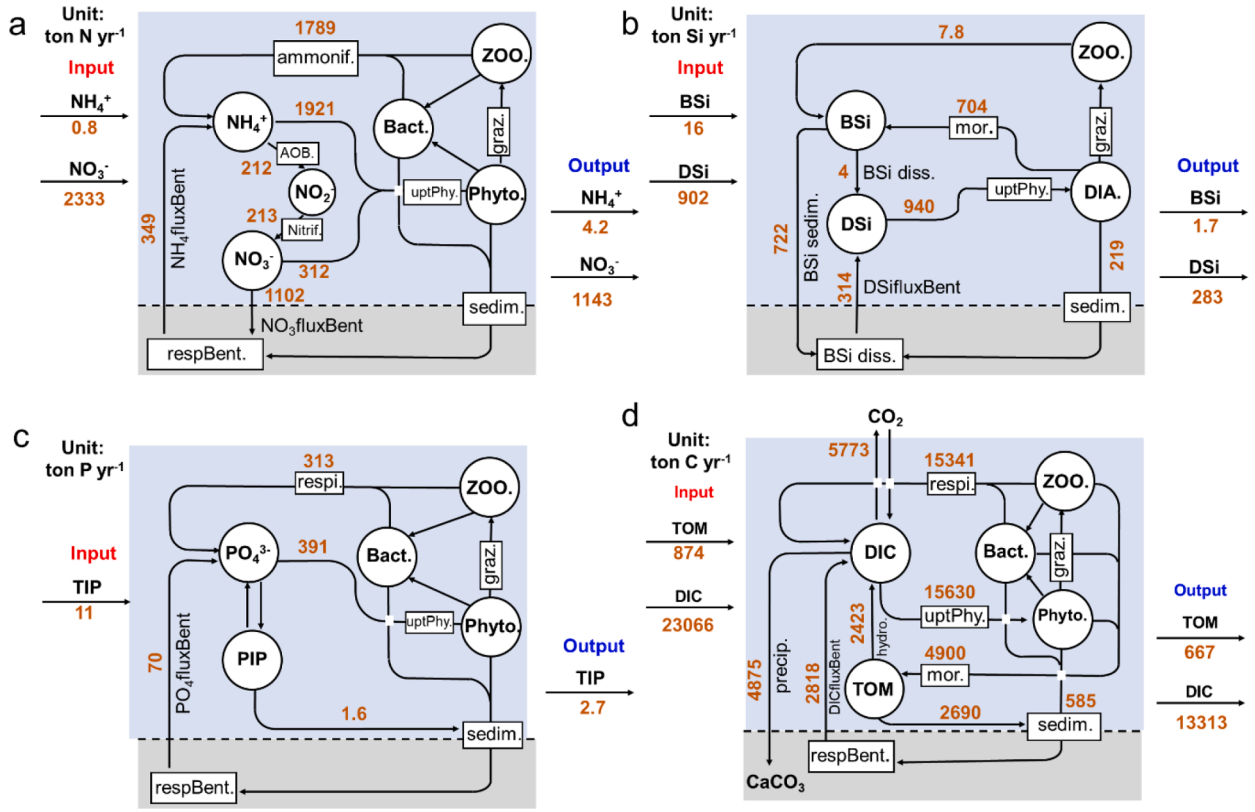

Fig. 6. Schematic diagram of the nutrients (a, b, c) and carbon (d) fate during one annual hydrological cycle (from December 2019 to November 2020) in the Marne Reservoir (detailed values for the three reservoirs are provided in Table S3). The imbalance between inputs and output is linked to retention/elimination and the initial/final state of the system (e.g., denitrification for NO_3^-).

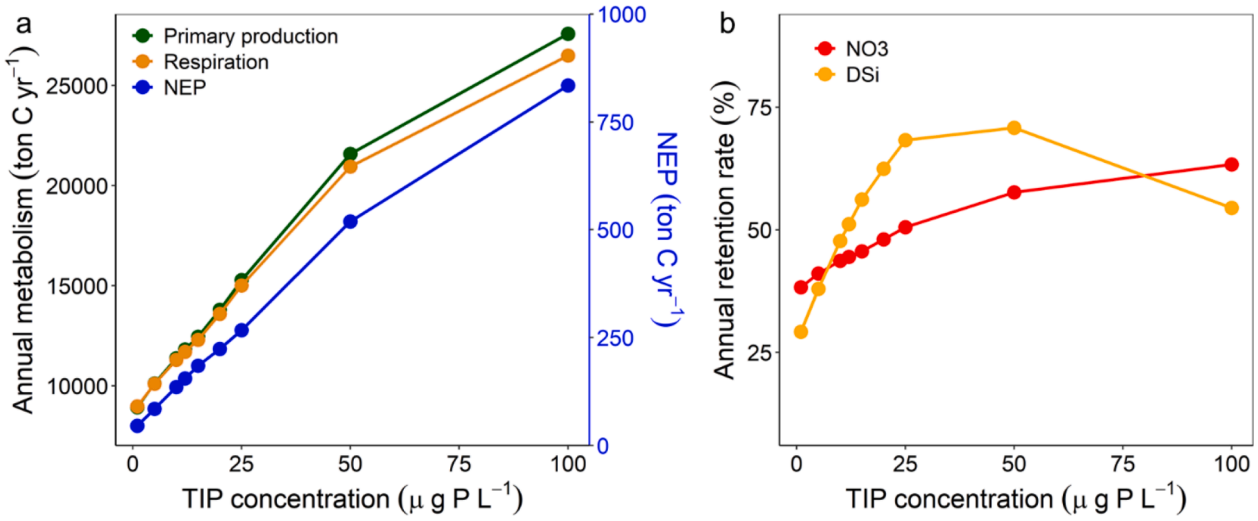

Fig. 7. Impact of the trophic state (increasing TIP concentrations) on the annual ecosystem metabolism, including (a) primary production and respiration, net ecosystem primary production (NEP = primary production – respiration) being shown on a 2nd Y-axis; and (b) retention rate of NO_3^- and DSi in the Marne Reservoir. All other boundary conditions are those of the annual hydrological cycle from December 2019 to November 2020. Note that the average TIP concentration flow into the reservoirs was approximately 20 μg P L^{-1} during 2019–2020.

(Aube–Amance) to 51% (Marne). The intensity of phytoplankton uptake (71–312 tons N yr^{-1}) and benthic denitrification (178–1102 tons N yr^{-1}), i.e., NO_3^- removal is clearly illustrated in Fig. 5 and Table S3. Ammonification (459–1789 tons N yr^{-1}) and phytoplankton uptake (520–2048 tons N yr^{-1}) were the main processes driving NH_4^+ transformations compared with NH_4^+ oxidation (48–213 tons N yr^{-1}) and benthic flux (80–349 tons N yr^{-1}). The three reservoirs showed high retention of DSi ranging from 49% (Aube–Temple) to 69% (Marne), and phytoplankton uptake (172–940 tons Si yr^{-1}) was the dominant process responsible for the DSi removal, sinking as BSi with diatom biomass, the three reservoirs also showed high BSi retention rates ranging from 38% (Aube–Temple) to 89% (Marne). In addition, 64%–79% of TIP was retained in the three reservoirs, with phytoplankton uptake of PO_4^{3-} being the dominant process retaining TIP in these reservoirs: from 98

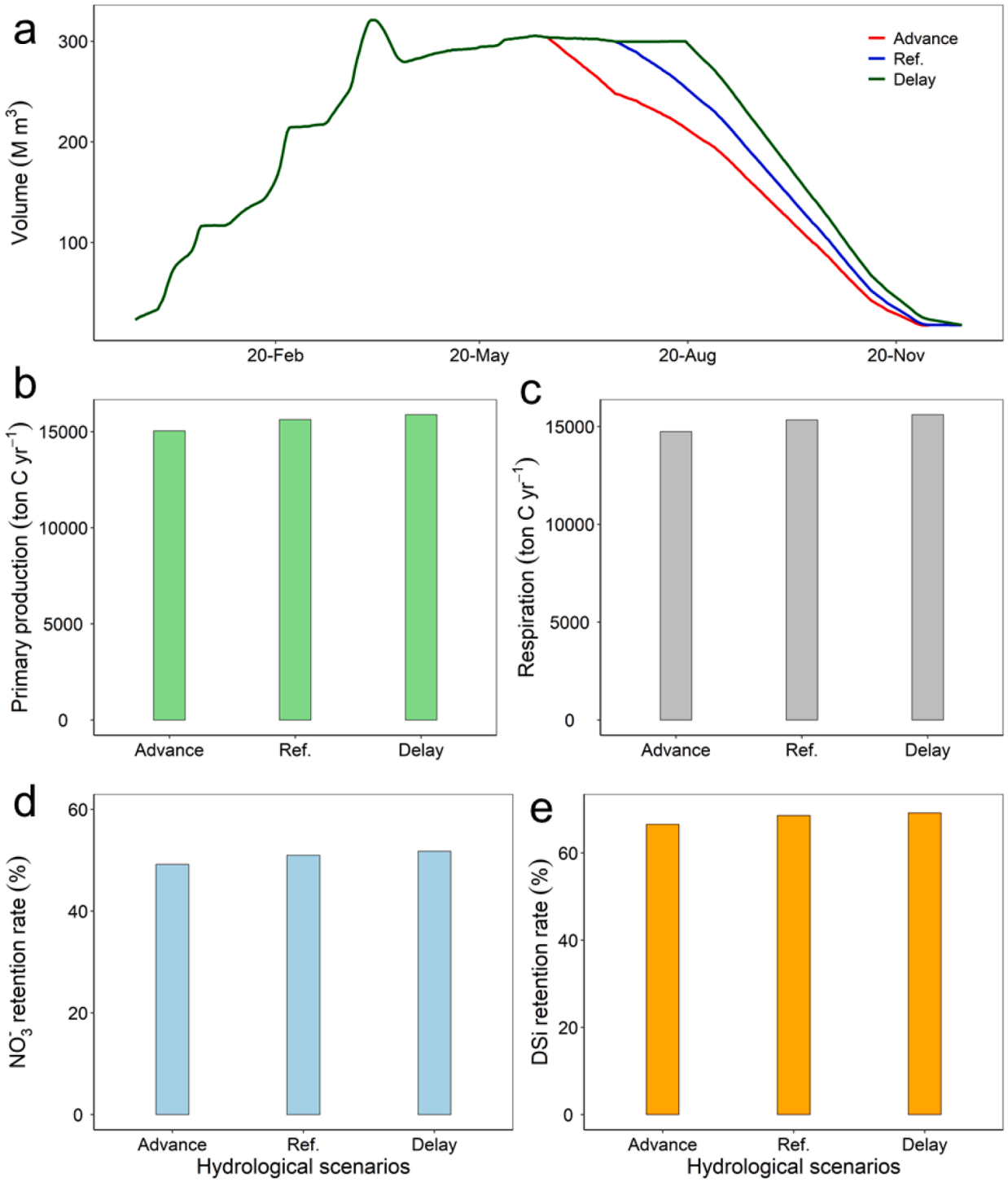

Fig. 8. Impact of three hydrological scenarios on (a) reservoir volume changes, (b) primary production, (c) respiration, (d) NO_3^- retention rate, and (e) DSi retention during during one hydrological cycle (from December 2019 to November 2020).

(Aube–Temple) to 391 (Marne) tons P yr^{-1}. In terms of DIC, the three reservoirs showed retention rates ranging from 25% (Aube–Amance) to 65% (Aube–Temple). The $CaCO_3$ precipitation (913–4875 tons C yr^{-1}) and CO_2 emission (859–5773 tons C yr^{-1}) were the most significant processes for DIC removal in the water column. Additionally, the annual net burial of TOC (total organic carbon) in sediments of the three reservoirs ranged from 61 (Aube–Temple) to 458 (Marne) tons C yr^{-1}.

3.3. Scenario analysis in the Marne reservoir

3.3.1. Assessing the impact of different trophic states

Primary production, respiration, and NEP all increased with TIP concentration in the inflowing river water, and their increasing rates were higher according to the range of TIP concentrations of 1–50 μg P L^{-1}. The gradual increases of NEP also indicated an increased

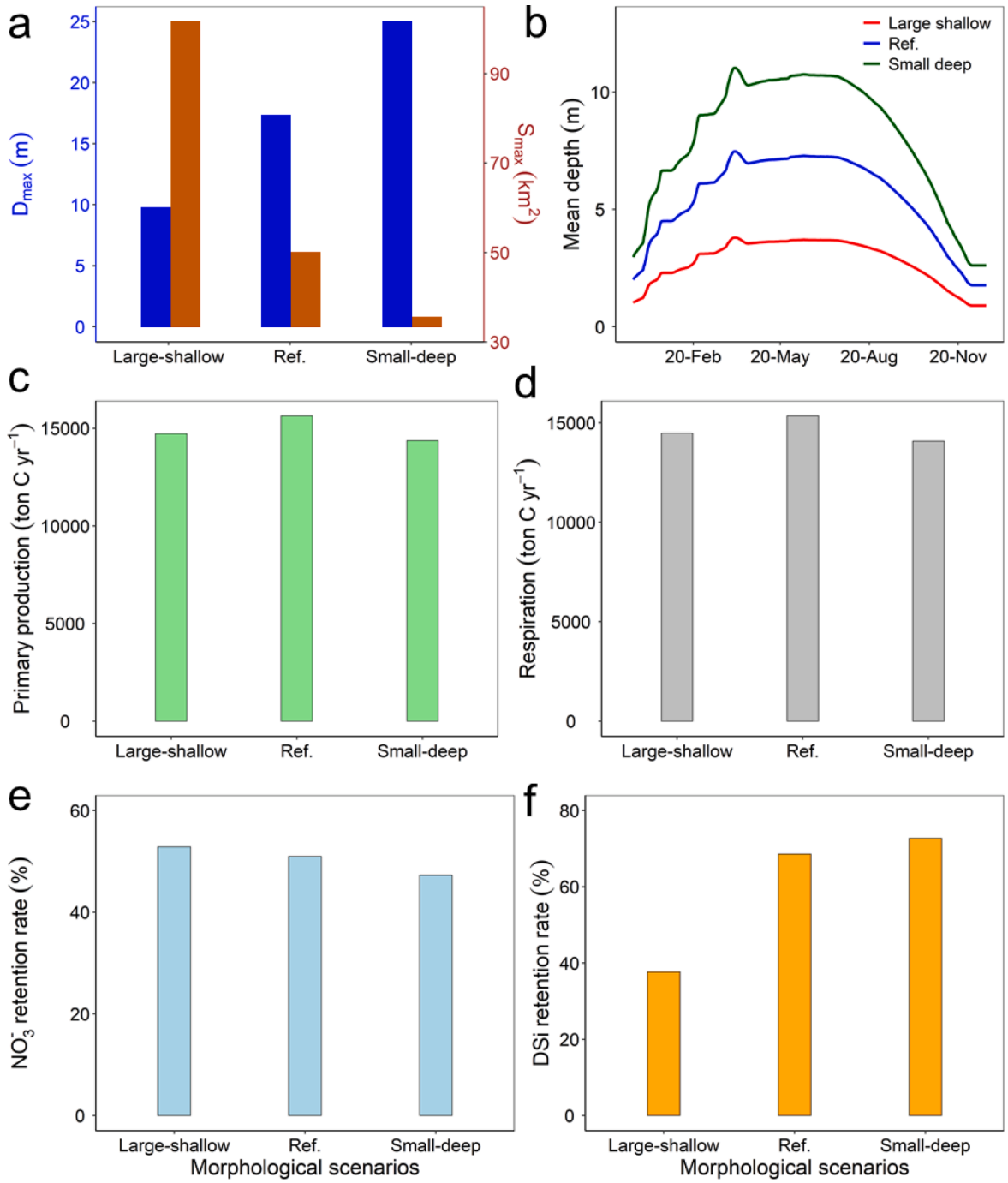

Fig. 9. Impacts of different morphologic parameters (a) D_{max} and S_{max} (see Text S1) of the Marne Reservoir on (b) calculated water column mean depth, (c) primary production, (d) respiration, (e) NO_3^- retention rate, and (f) DSi retention rate during one hydrological cycle (from December 2019 to November 2020).

autotrophy with increasing TIP concentrations (Fig. 7a). In addition, the trophic state of the reservoir significantly impacted the retention of NO_3^- and DSi. The retention rate of NO_3^- showed an increase from 38% (1 μg P L^{-1}) to 63% (100 μg P L^{-1}), but this increase of the NO_3^- retention rate was the highest (from 38% to 51%) in the lower range of the TIP concentrations explored (1–25 μg P L^{-1}) (Fig. 7b). The retention rate of DSi was greater in response to the increasing TIP concentrations of 1–25 μg P L^{-1} (from 29% to 68%), with a slight decrease from 70% to 54% as the TIP loads continued to increase from 50 to 100 μg P L^{-1} (Fig. 7b).

3.3.2. *Changes in hydrological management strategies*

Without significantly affecting the primary function of the Marne Reservoir (i.e., to prevent flooding and support water flow), the changes in hydrological management strategies involve advancing or delaying for 1 month the start of the emptying period in the reservoir (Fig. 8). Compared with the reference scenario, primary production and respiration showed similar patterns with values, respectively, of only 1.6% and 1.7% higher in the delayed hydrological scenario and of −3.8% and −3.9%, i.e., lower, in the advanced scenario (Fig. 8b, c). Regarding

retention rates, those of NO_3^- decreased only slightly by 2% (Advanced) and increased by 1% (Delayed) (Fig. 8d). Similarly, the DSi retention did not change (Delayed) or did so by only −2% (Advanced) (Fig. 8e). Overall, the ecosystem metabolism and nutrient retention did not change significantly under these possible modifications of the hydrological management strategies for the Marne Reservoir.

3.3.3. Different morphological characteristics in the Marne Reservoir

Changes in morphological parameters (maximum depth and maximum surface) that were used to define the idealized spherical shape of the reservoir logically had strong impacts on the mean depths of the water column calculated daily according to hydrological conditions (Fig. 9). The ecosystem metabolism changed only slightly. Compared with the reference situation, primary production and respiration decreased, respectively, by 5.8% and 5.6% for the large–shallow scenario; similarly, lower percentages of both primary production and respiration were obtained for the small–deep scenario (−8% and −8.3%, respectively) relative to the reference (Fig. 9b, c). For the nutrient retention rates, the large–shallow reservoir showed a slight increased NO_3^- retention rate (from 51% -Ref.- to 53%) and a small decreased rate (from 51% -Ref.- to 47%) for the small–deep scenario (Fig. 9d). However, the low DSi retention rate was significantly lowered in the large–shallow reservoir (from 69% -Ref.- to 38%), while it only increased marginally (from 69% -Ref.- to 73%) for the small–deep reservoir (Fig. 9e). In addition, we further found that the benthic denitrification (1140 tons N yr^{-1}) and benthic flux of DSi (390 tons Si yr^{-1}) in the large–shallow reservoir were 1.1 and 1.6 times higher than the small–deep reservoir, respectively (Fig. S13). Although primary production in the large–shallow scenario was slightly higher than in the small–deep scenario, the DSi assimilation was, nevertheless, 1.2 times lower than in the latter.

4. Discussion

4.1. Evaluation of the model: performance and limitations

Overall, the Barman model showed satisfactory simulation results for the key water quality variables and CO_2 dynamics during 2019–2020 in the three reservoirs of the Seine Basin, despite some discrepancies (Figs. 2 and S5–S7). In the three reservoirs, the peak value of Chl-*a* was generally observed during the end of the emptying period when water levels are relatively low, which may enhance the nutrient exchanges from the sediment to the water column, increase light availability, and thereby stimulate the development of phytoplankton in reservoirs (see Yan et al., 2022). For NO_3^- concentrations, the lowest values were also observed with low water depth, which were not fully captured by the model. A possible explanation is that the resuspension process that increases SM concentrations in the water column when water levels are low was not considered in the model, while the concentration of SM has been shown to significantly influence the denitrification process in aquatic ecosystems (e.g., Jia et al., 2016; Xia et al., 2017). Moreover, although stratification could occasionally occur during summer when temperature and water level were high in these reservoirs (see Garnier et al., 2000), the zero-dimension Barman model in fact does not consider such stratification but assumes that the three reservoirs are well-mixed systems. The Barman model, which needs fewer input data and lesser running time than multi-dimension models (e.g., the Delft3D and CE-QUAL-W2 models) (Lindenschmidt et al., 2019; Wu et al., 2022), fails to reproduce possible low oxygen concentrations in bottom waters, suitable for denitrification processes. Nevertheless, the model captured fairly well the dynamics of NO_3^- and other variables (e.g., nutrients) in the water column, which shows its usefulness in simulating biogeochemical processes in these reservoirs.

For the simulation of the variations in CO_2 concentrations, the gas transfer coefficient (k_{600}) plays an important role in simulating CO_2 in the three reservoirs (e.g., in the Marne Reservoir, Fig. S14). In this study, the daily wind speed was not available, and we used monthly average wind speed in a single location and selected a k_{600} constant value of 0.08 m h^{-1} (median value calculated from six different methods, see Text S5). Given the importance of gas transfer velocity (k) for modeling the CO_2 dynamics, we believe that the high-resolution measurement of k is needed in future studies. Additionally, we have only estimated the precipitation and dissolution rates of $CaCO_3$ (see Text S4) based on seven dates in the three reservoirs during 2020. Despite the satisfactory simulation results of TA and DIC found in the Marne, Seine, and Aube (Lake Temple) reservoirs, specific research efforts are still required focusing on the precipitation and dissolution rates of $CaCO_3$ in these reservoirs with generic kinetics equations in a future version of Barman model.

4.2. Nutrients in reservoirs: budgets and transformations

Nutrient budgets in the three reservoirs were estimated using a mass balance method based on the uneven temporal frequency measurements (bimonthly, monthly, and seasonal) during 1993–1995 (Garnier et al., 1999) and 1998–2018 (Yan et al., 2021b), which indicated that reservoirs play an important role in nutrient retention, whatever the measurement strategy. In this study, the biogeochemical processes responsible for the nutrient transformations were analyzed with the Barman model, and the nutrient retention rates were thus calculated based on simulations at a daily time step. Our results are consistent with previous findings, demonstrating that reservoirs exhibit a strong capacity for retention of DIC and nutrients (N, P, Si) (Akbarzadeh et al., 2019; Maavara et al., 2017, 2015b, 2014; Mendonça et al., 2017), and they are also close to our previous long-term assessments using monthly or seasonal measurements during 1998–2018 (Yan et al., 2021b). Uneven and low-frequency measurements may not capture the seasonal patterns of nutrient concentrations in water, and thereby lead to uncertainty in evaluating their budgets (see Kong et al., 2019 for NO_3^-). However, the different data series gathered from these reservoirs showed similar retention rates according to our previous study (Yan et al., 2021b), which would support our simulation results. High-frequency measurements are well adapted for NEP determination, but probe availability for establishing the nutrient budgets of interest is still limited, and the maintenance of probes for frequent or continuous measurements is costly. Although several statistical models have been used for nutrient retention rates in lakes and reservoirs, including N (Alexander et al., 2002; Harrison et al., 2009; Seitzinger et al., 2002) and Si (Maavara et al., 2014), the underlying biological processes could not be fully described. Based on the mechanistic Barman model (i.e., process-based), which describes the major processes involved in the biogeochemical transformations of C and nutrients (see SI TextS1, Fig. S2), we could explicitly unravel both the fate of carbon and nutrients and the importance of physical processes in the three reservoirs (see 3.2.3). Therefore, our results would provide a deep understanding of seasonal variations in water quality variables in these reservoirs, and also a potential utility to minimize the impact of the reservoirs on their downstream water quality.

4.3. Effects of external phosphorus management on reservoir ecological function

Taking the Marne Reservoir as an example, the response of the ecosystem metabolism to the external P loads clearly revealed the importance of P concentrations in the primary production, respiration, and NEP. It is well known that primary production combines the biogeochemical cycles of C and nutrients in aquatic ecosystems (Bernhardt, 2013). Interestingly, our results indicated that the retention efficiency of NO_3^- and DSi varied with the external P loads. For NO_3^- retention, denitrification (dominantly in the sediment) was shown to be the main process responsible for NO_3^- elimination in the three reservoirs (see 3.2.2). In addition to the levels of DO and NO_3^-, the availability of

biodegradable organic matter is one of the factors controlling denitrification rates (Seitzinger et al., 2006). Therefore, at low P concentration, low phytoplankton biomass was supported and less organic matter fell to the sediment, thus ultimately limiting the denitrification rate and thereby lowering the NO_3^- retention rate in the reservoirs (Bernhardt, 2013; Finlay et al., 2013).

Similarly, the elimination of DSi was mainly induced by diatom uptake, which was significantly affected by DIP concentrations in the reservoirs (Maavara et al., 2015a; Xiao et al., 2019). Increasing P concentrations in the range of 1–25 μg P L^{-1} stimulates the development of diatoms in the Marne Reservoir, and thus DSi uptake. Without other limitations, the growth of diatoms would increase with P concentrations; however, other groups of phytoplankton (non-diatoms) show a greater competitive advantage than diatoms in freshwaters with high P concentrations (Burson et al., 2018), which may further impact the uptake and retention rate of DSi in reservoirs. For instance, the biomass of diatoms, as calculated by the model, was essentially constant for P loads ranging from 25 to 50 μg P L^{-1} and levelled off or decreased instead when P loads exceeded 50 μg P L^{-1} (see Text S6, Fig. S15), which resulted in a reduced DSi retention efficiency when the TIP concentration exceeded 50 μg P L^{-1}.

This result confirms that changes in DIP concentrations clearly affect biogeochemical processes. On the one hand, denitrification (and NO_3^- retention) may be reduced at low P concentrations, without playing a positive role in removing NO_3^- for downstream rivers. On the other hand, increasing DIP may lead to an undesirable change in phytoplankton composition from diatoms to non-diatoms, the latter being often unpalatable for zooplankton or is even toxic. Overall, the response of the biogeochemical processes (e.g., metabolism) and ecological functions (e.g., nutrient retention) to external P loads explored here provided new insight into the impact of the reservoir on downstream nutrient concentrations, a topic of great interest, especially for the Seine River water quality, which is mainly used to produce drinking water for the 12 M inhabitants of the Paris conurbation (Flipo et al., 2021).

4.4. Implications of hydrological management strategies and morphological characteristics for reservoir water quality

The fluctuation in water levels induced by the hydrological management strategies is one of the typical features of reservoirs, and has been recognized to impact biogeochemical processes (Geraldes and Boavida, 2005). In this study, advancing the emptying period by 1 month (i.e., in June) could support downstream low water flows earlier at the end of spring, whereas delaying the water release would maintain high water levels in the reservoirs for recreational activities in summer. We found that changing hydrological management strategies only slightly impacts the ecosystem metabolism and the retention of NO_3^- and DSi in the Marne Reservoir, due to the fact that the concentrations of NO_3^- and DSi were already low in June. Several studies have explored the impact of hydrological management strategies on downstream water quality, such as water temperature, DO, and nutrient concentrations, which, however, mainly focused on optimizing the withdrawal depth of the dam (e.g., Calamita et al., 2021; Sadeghian et al., 2015). In contrast to most large reservoirs in the world, the three reservoirs of the Seine River system are diverted from their related rivers and connected with them by artificial canals, rather than being constructed by damming a river. Thanks to a few SGL' measurements in the canals and in the reservoirs, we assumed the impact of the canals to be low so that downstream changes in the rivers is due to changes in the reservoirs.

Interestingly, we found that modifying the mean depth of a reservoir without modifying the hydrological management strategy can play a role in the nutrient retention efficiency. Indeed, a shallower reservoir showed a 6% higher NO_3^- retention rate than a deeper reservoir, but a significantly lower (35%) DSi retention rate (Fig. 9). With the same volume, the shallow reservoir has a higher area of sediment interacting with the overlying thinner water column, which has been considered as the critical attribute regulating in-lake nutrient biogeochemical cycles (Qin et al., 2020). Denitrification is the dominant process resulting in NO_3^- elimination in the reservoirs, which is determined by the availability of NO_3^-, biodegradable organic matter, and anaerobic/aerobic conditions (Seitzinger et al., 2006). In this study, although primary production in the shallow scenario was 5.8% lower than the reference scenario, benthic denitrification was higher than the latter (Fig. S13). DSi retention in the reservoir is the net result of the interactions between several biogeochemical processes, including external input of Si, in-reservoir formation of BSi, and dissolution and burial of BSi (Lauerwald et al., 2013; Maavara et al., 2015a; Teodoru et al., 2006). Here, we found that a shallower-shaped reservoir favored a high DSi flux from benthic release to the water column and relatively lower uptake in the water column (Fig. S13), which led to a low DSi retention efficiency. Thus, when combining the benthic fluxes of NO_3^- and DSi, the reservoir with lower mean depth potentially enhances nutrient exchanges at the water and sediment interface, and further impacts the nutrient retention efficiencies.

5. Conclusions

The Barman model was successfully applied to the three diverted reservoirs of the Seine Basin, demonstrating its ability to reproduce the seasonal variations both of the nutrients and the CO_2 concentrations. The biogeochemical processes and nutrient fate were systematically analyzed and quantified for each of the three reservoirs, we found that:

1 the three reservoirs are autotrophic ecosystems and showed high removal efficiency of C and nutrient during 2019-2020.
2 benthic denitrification is the most significant process accounting for NO_3^- elimination; diatom uptake is the key process for DSi elimination; precipitation and dissolution of $CaCO_3$ and CO_2 emissions are dominant drivers for the decrease in DIC; and the assimilation of PO_4^{3-} by phytoplankton uptake represents the main source of retention of TIP.
3 trophic state and mean water depth of reservoirs impact the biogeochemical processes and the retention efficiency of NO_3^- and DSi based on scenarios analysis results.

Overall, this study unravels the fate of C and nutrients in the three reservoirs based on the Barman model, and scenario results provide useful references for the management of water quality in reservoirs and the potential impact on downstream rivers.

Declaration of Competing Interest

The authors declare that they have no known competing financial interest or personal relationships that could have appeared to influence the work reported in this paper.

Data availability

Data will be made available on request.

Acknowledgments

We thank Benjamin Mercier, Sébastien Bosc, Anunciacion Martinez Serrano, and Romane Nespoulet for their assistance in the field with sampling and with chemical analysis in the laboratory. We thank Thomas Guillon (former master degree student) for having formalized the equation describing the idealized shape of the reservoirs. We would also like to thank the Seine Grands Lacs for providing hydrological data. Xingcheng Yan's PhD is funded by China Scholarship Council (CSC, No. 201806860053) and ASDB from Sorbonne University within the framework of the PIREN Seine program (Programme Interdisciplinaire

de Recherche sur l'ENvironnement du bassin de la Seine, https://www.piren-seine.fr/). Finally, Xingcheng Yan is pleased to thank Yang Su for her encouragement during his study.

Supplementary materials

Supplementary material associated with this article can be found, in the online version, at doi:10.1016/j.watres.2022.119135.

References

Abril, G., Bouillon, S., Darchambeau, F., Teodoru, C.R., Marwick, T.R., Tamooh, F., Ochieng Omengo, F., Geeraert, N., Deirmendjian, L., Polsenaere, P., Borges, A.V., 2015. Technical note: large overestimation of pCO_2 calculated from pH and alkalinity in acidic, organic-rich freshwaters. Biogeosciences 12, 67–78. https://doi.org/10.5194/bg-12-67-2015.

Akbarzadeh, Z., Maavara, T., Slowinski, S., Van Cappellen, P., 2019. Effects of damming on river nitrogen fluxes: a global analysis. Glob. Biogeochem. Cycles 33, 1339–1357. https://doi.org/10.1029/2019GB006222.

Alexander, R.B., Elliott, A.H., Shankar, U., McBride, G.B., 2002. Estimating the sources and transport of nutrients in the Waikato River Basin, New Zealand. Water Resour. Res. 38 https://doi.org/10.1029/2001WR000878, 4–1.

Bastviken, D., Tranvik, L.J., Downing, J.A., Crill, P.M., Enrich-Prast, A., 2011. Freshwater methane emissions offset the continental carbon sink. Science (80-.) 331, 50. https://doi.org/10.1126/science.1196808.

Bernhardt, E.S., 2013. Cleaner lakes are dirtier lakes. Science (80-.) 342, 205–206. https://doi.org/10.1126/SCIENCE.1245279.

Billen, G., Garnier, J., Hanset, P.H., 1994. Modelling phytoplankton development in whole drainage networks : the Riverstrahler model applied to the Seine river system. Hydrobiologia 289, 119–137.

Billen, G., Garnier, J., Némery, J., Sebilo, M., Sferratore, A., Barles, S., Benoit, P., Benoît, M., 2007. A long-term view of nutrient transfers through the Seine river continuum. Sci. Total Environ. 375, 80–97. https://doi.org/10.1016/j.scitotenv.2006.12.005.

Billen, G., Garnier, J., Silvestre, M., 2015. A simplified algorithm for calculating benthic nutrient fluxes in river systems. Ann. Limnol. 51, 37–47. https://doi.org/10.1051/limn/2014030.

Bonnet, M.P., Poulin, M., 2004. DyLEM-1D: a 1D physical and biochemical model for planktonic succession, nutrients and dissolved oxygen cycling: application to a hyper-eutrophic reservoir. Ecol. Model. 180, 317–344. https://doi.org/10.1016/J.ECOLMODEL.2004.04.037.

Bouwman, L., Goldewijk, K.K., Van Der Hoek, K.W., Beusen, A.H.W., Van Vuuren, D.P., Willems, J., Rufino, M.C., Stehfest, E., 2013. Exploring global changes in nitrogen and phosphorus cycles in agriculture induced by livestock production over the 1900-2050 period. Proc. Natl. Acad. Sci. U. S. A. 110, 20882–20887. https://doi.org/10.1073/PNAS.1012878108/SUPPL_FILE/PNAS.201012878SI.PDF.

Burson, A., Stomp, M., Greenwell, E., Grosse, J., Huisman, J., 2018. Competition for nutrients and light: testing advances in resource competition with a natural phytoplankton community. Ecology 99, 1108–1118. https://doi.org/10.1002/ECY.2187.

Calamita, E., Vanzo, D., Wehrli, B., Schmid, M., 2021. Lake modeling reveals management opportunities for improving water quality downstream of transboundary tropical dams. Water Resour. Res. 57 https://doi.org/10.1029/2020WR027465 e2020WR027465.

Chen, Q., Shi, W., Huisman, J., Maberly, S.C., Zhang, J., Yu, J., Chen, Y., Tonina, D., Yi, Q., 2020. Hydropower reservoirs on the upper Mekong River modify nutrient bioavailability downstream. Natl. Sci. Rev. https://doi.org/10.1093/nsr/nwaa026.

Chen, Z., Huang, P., Zhang, Z., 2019. Interaction between carbon dioxide emissions and eutrophication in a drinking water reservoir: a three-dimensional ecological modeling approach. Sci. Total Environ. 663, 369–379. https://doi.org/10.1016/j.scitotenv.2019.01.336.

Cole, J.J., Prairie, Y.T., Caraco, N.F., McDowell, W.H., Tranvik, L.J., Striegl, R.G., Duarte, C.M., Kortelainen, P., Downing, J.A., Middelburg, J.J., Melack, J., 2007. Plumbing the global carbon cycle: integrating inland waters into the terrestrial carbon budget. Ecosystems 10, 171–184. https://doi.org/10.1007/s10021-006-9013-8.

Deemer, B.R., Harrison, J.A., Li, S., Beaulieu, J.J., Delsontro, T., Barros, N., Bezerra-Neto, J.F., Powers, S.M., Dos Santos, M.A., Vonk, J.A., 2016. Greenhouse gas emissions from reservoir water surfaces: a new global synthesis. Bioscience 66, 949–964. https://doi.org/10.1093/biosci/biw117.

Finlay, J.C., Small, G.E., Sterner, R.W., 2013. Human influences on nitrogen removal in lakes. Science (80-.) 342, 247–250. https://doi.org/10.1126/SCIENCE.1242575/SUPPL_FILE/FINLAY.SM.PDF.

Flipo, N., Lestel, L., Labadie, P., Meybeck, M., Garnier, J., 2021. Trajectories of the seine river basin [WWW Document]. Handb. Environ. Chem. https://doi.org/10.1007/698_2019_437.

Friedl, G., Wüest, A., 2002. Disrupting biogeochemical cycles - consequences of damming. Aquat. Sci. https://doi.org/10.1007/s00027-002-8054-0.

Garnier, J., Billen, G., Hannon, E., Fonbonne, S., Videnina, Y., Soulie, M., 2002. Modelling the transfer and retention of nutrients in the drainage network of the Danube river. Estuar. Coast. Shelf Sci. 54, 285–308. https://doi.org/10.1006/ecss.2000.0648.

Garnier, J., Billen, G., Sanchez, N., Leporcq, B., 2000. Ecological functioning of the Marne reservoir (upper Seine basin, France). Regul. River. Res. Manag. 16, 51–71. https://doi.org/10.1002/(sici)1099-1646(200001/02)16, 1<51::aid-rrr571>3.3.co;2-9.

Garnier, J., Leporcq, B., Sanchez, N., Philippon, X., 1999. Biogeochemical mass-balances (C, N, P, Si) in three large reservoirs of the Seine Basin (France). Biogeochemistry 47, 119–146. https://doi.org/10.1023/A:1006101318417.

Garnier, J., Marescaux, A., Guillon, S., Vilmin, L., Rocher, V., Billen, G., Thieu, V., Silvestre, M., Passy, P., Raimonet, M., Groleau, A., Théry, S., Tallec, G., Flipo, N., 2021. Ecological Functioning of the Seine River: From Long-Term Modelling Approaches to High-Frequency Data Analysis, in: Handbook of Environmental Chemistry. Springer, Berlin, Heidelberg, pp. 189–216. https://doi.org/10.1007/698_2019_379 bll.

Geraldes, A.M., Boavida, M.J., 2005. Seasonal water level fluctuations: implications for reservoir limnology and management. Lakes Reserv. Res. Manag. 10, 59–69. https://doi.org/10.1111/J.1440-1770.2005.00257.X.

Grizzetti, B., Vigiak, O., Udias, A., Aloe, A., Zanni, M., Bouraoui, F., Pistocchi, A., Dorati, C., Friedland, R., De Roo, A., Benitez Sanz, C., Leip, A., Bielza, M., 2021. How EU policies could reduce nutrient pollution in European inland and coastal waters. Glob. Environ. Chang. 69, 102281 https://doi.org/10.1016/J.GLOENVCHA.2021.102281.

Harrison, J.A., Maranger, R.J., Alexander, R.B., Giblin, A.E., Jacinthe, P.A., Mayorga, E., Seitzinger, S.P., Sobota, D.J., Wollheim, W.M., 2009. The regional and global significance of nitrogen removal in lakes and reservoirs. Biogeochemistry 93, 143–157. https://doi.org/10.1007/s10533-008-9272-x.

Harrison, J.A., Prairie, Y.T., Mercier-Blais, S., Soued, C., 2021. Year-2020 global distribution and pathways of reservoir methane and carbon dioxide emissions according to the greenhouse gas from reservoirs (G-res) model. Glob. Biogeochem. Cycle. 35 https://doi.org/10.1029/2020GB006888 e2020GB006888.

Hirsch, R.M., Moyer, D.L., Archfield, S.A., 2010. Weighted regressions on time, discharge, and season (WRTDS), with an application to Chesapeake Bay River Inputs. J. Am. Water Resour. Assoc. 46, 857. https://doi.org/10.1111/J.1752-1688.2010.00482.X.

Jia, Z., Liu, T., Xia, X., Xia, N., 2016. Effect of particle size and composition of suspended sediment on denitrification in river water. Sci. Total Environ. 541, 934–940. https://doi.org/10.1016/j.scitotenv.2015.10.012.

Jones, M.N., 1984. Nitrate reduction by shaking with cadmium: alternative to cadmium columns. Water Res. 18, 643–646. https://doi.org/10.1016/0043-1354(84)90215-X.

Kong, X., Zhan, Q., Boehrer, B., Rinke, K., 2019. High frequency data provide new insights into evaluating and modeling nitrogen retention in reservoirs. Water Res. 166, 115017 https://doi.org/10.1016/J.WATRES.2019.115017.

Lauerwald, R., Hartmann, J., Moosdorf, N., Dürr, H.H., Kempe, S., 2013. Retention of dissolved silica within the fluvial system of the conterminous USA. Biogeochemistry 112, 637–659. https://doi.org/10.1007/S10533-012-9754-8/FIGURES/5.

Li, J., Pu, J., Zhang, T., 2022. Transport and transformation of dissolved inorganic carbon in a subtropical groundwater-fed reservoir, south China. Water Res. 209, 117905 https://doi.org/10.1016/J.WATRES.2021.117905.

Lindenschmidt, K.E., Carr, M.K., Sadeghian, A., Morales-Marin, L., 2019. CE-QUAL-W2 model of dam outflow elevation impact on temperature, dissolved oxygen and nutrients in a reservoir. Sci. Data 6, 1–7. https://doi.org/10.1038/s41597-019-0316-y, 2019 61.

Lorenzen, C.J., 1967. Determination of chlorophyll and pheo-pigments: spectrophotometric equations. Limnol. Oceanogr. https://doi.org/10.4319/lo.1967.12.2.0343.

Maavara, T., Akbarzadeh, Z., Van Cappellen, P., 2020a. Global dam-driven changes to riverine N:P:Si ratios delivered to the coastal ocean. Geophys. Res. Lett. 47 https://doi.org/10.1029/2020GL088288.

Maavara, T., Chen, Q., Van Meter, K., Brown, L.E., Zhang, J., Ni, J., Zarfl, C., 2020b. River dam impacts on biogeochemical cycling. Nat. Rev. Earth Environ. 1, 103–116. https://doi.org/10.1038/s43017-019-0019-0.

Maavara, T., Dürr, H.H., Van Cappellen, P., 2014. Worldwide retention of nutrient silicon by river damming: from sparse data set to global estimate. Glob. Biogeochem. Cycle 28, 842–855. https://doi.org/10.1002/2014GB004875.

Maavara, T., Hood, J.L.A., North, R.L., Doig, L.E., Parsons, C.T., Johansson, J., Liber, K., Hudson, J.J., Lucas, B.T., Vandergucht, D.M., Van Cappellen, P., 2015a. Reactive silicon dynamics in a large prairie reservoir (Lake Diefenbaker, Saskatchewan). J. Great Lakes Res. 41, 100–109. https://doi.org/10.1016/j.jglr.2015.04.003.

Maavara, T., Lauerwald, R., Regnier, P., Van Cappellen, P., 2017. Global perturbation of organic carbon cycling by river damming. Nat. Commun. 8, 15347. https://doi.org/10.1038/ncomms15347.

Maavara, T., Parsons, C.T., Ridenour, C., Stojanovic, S., Dürr, H.H., Powley, H.R., Van Cappellen, P., 2015b. Global phosphorus retention by river damming. Proc. Natl. Acad. Sci. U. S. A. 112, 15603–15608. https://doi.org/10.1073/pnas.1511797112.

Marescaux, A., Thieu, V., Borges, A.V., Garnier, J., 2018. Seasonal and spatial variability of the partial pressure of carbon dioxide in the human-impacted Seine River in France. Sci. Rep. 8 https://doi.org/10.1038/s41598-018-32332-2.

Marescaux, A., Thieu, V., Gypens, N., Silvestre, M., Garnier, J., 2020. Modeling inorganic carbon dynamics in the seine river continuum in France. Hydrol. Earth Syst. Sci. 24, 2379–2398. https://doi.org/10.5194/hess-24-2379-2020.

Mendonça, R., Müller, R.A., Clow, D., Verpoorter, C., Raymond, P., Tranvik, L.J., Sobek, S., 2017. Organic carbon burial in global lakes and reservoirs. Nat. Commun. 8, 1–6. https://doi.org/10.1038/s41467-017-01789-6.

Mooij, W.M., Trolle, D., Jeppesen, E., Arhonditsis, G., Belolipetsky, P.V., Chitamwebwa, D.B.R., Degermendzhy, A.G., DeAngelis, D.L., De Senerpont Domis, L.N., Downing, A.S., Elliott, J.A., Fragoso, C.R., Gaedke, U., Genova, S.N., Gulati, R.D., Håkanson, L., Hamilton, D.P., Hipsey, M.R., t Hoen, J., Hülsmann, S.,

Los, F.H., Makler-Pick, V., Petzoldt, T., Prokopkin, I.G., Rinke, K., Schep, S.A., Tominaga, K., van Dam, A.A., van Nes, E.H., Wells, S.A., Janse, J.H., 2010. Challenges and opportunities for integrating lake ecosystem modelling approaches. Aquat. Ecol. 443 (44), 633–667. https://doi.org/10.1007/S10452-010-9339-3, 2010.

Némery, J., Garnier, J., Morel, C., 2005. Phosphorus budget in the Marne Watershed (France): urban vs. diffuse sources, dissolved vs. particulate forms. Biogeochem 721 (72), 35–66. https://doi.org/10.1007/S10533-004-0078-1, 2005.

Pierrot, D.E., Lewis, E., Wallace, D.W.R., 2006. MS Excel program developed for CO2 system calculations. Carbon Dioxide Information Analysis Center, Oak Ridge National Laboratory, US Department of Energy [WWW Document]. Ornl/Cdiac-Ios. URL https://cdiac.ess-dive.lbl.gov/ftp/co2sys/CO2SYS_calc_XLS_v2.1/?C=N;O=A (toegang verkry 11.26.19).

Qin, B., Zhou, J., Elser, J.J., Gardner, W.S., Deng, J., Brookes, J.D., 2020. Water Depth Underpins the Relative Roles and Fates of Nitrogen and Phosphorus in Lakes. Environ. Sci. Technol. 54, 3191–3198. https://doi.org/10.1021/ACS.EST.9B05858/SUPPL_FILE/ES9B05858_SI_002.XLSX.

Rodier, J., 1984. L'analyse de l'eau, 7ème édition. Dunot, Paris (France) (Ed).

Sadeghian, A., Chapra, S.C., Hudson, J., Wheater, H., Lindenschmidt, K.E., 2018. Improving in-lake water quality modeling using variable chlorophyll a/algal biomass ratios. Environ. Model. Softw. 101, 73–85. https://doi.org/10.1016/J.ENVSOFT.2017.12.009.

Sadeghian, A., de Boer, D., Hudson, J.J., Wheater, H., Lindenschmidt, K.E., 2015. Lake Diefenbaker temperature model. J. Great Lakes Res. 41, 8–21. https://doi.org/10.1016/J.JGLR.2015.10.002.

Schmutz, S., Moog, O., 2018. Dams: ecological impacts and management. Riverine Ecosyst. Manag. 111–127. https://doi.org/10.1007/978-3-319-73250-3_6.

Seitzinger, S., Harrison, J.A, Böhlke, J.K., Bouwman, A.F., Lowrance, R., Peterson, B., Tobias, C., Drecht, G, Van, 2006. Denitrification across landscapes and waterscapers: a synthesis. Ecol. Appl. 16, 2064–2090. https://doi.org/10.1890/1051-0761 (2006)016[2064:DALAWA]2.0.CO;2.

Seitzinger, S.P., Styles, R.V., Boyer, E.W., Alexander, R.B., Billen, G., Howarth, R.W., Mayer, B., Van Breemen, N., 2002. Nitrogen retention in rivers: model development and application to watersheds in the northeastern U.S.A. Biogeochem 571 (57), 199–237. https://doi.org/10.1023/A:1015745629794, 2002.

Slawyk, G., MacIsaac, J.J., 1972. Comparison of two automated ammonium methods in a region of coastal upwelling. Deep Sea Res. Oceanogr. Abstr. 19, 521–524. https://doi.org/10.1016/0011-7471(72)90019-8.

Stumm, W., Morgan, J.J., 1996. Aquatic chemistry: chemical equilibria and rates in natural waters. John Wiley & Sons. https://doi.org/10.5860/choice.33-6312.

Teodoru, C., Dimopoulos, A., Wehrli, B., 2006. Biogenic silica accumulation in the sediments of Iron Gate I Reservoir on the Danube River. Aquat. Sci. 469–481. https://doi.org/10.1007/S00027-006-0822-9, 2006 684 68.

Thieu, V., Guillon, T., Billen, G., Garnier, J., Thouvenot, M., 2006. Applicatif BARMAN Notice d'utilisation-Juillet 2006. Rapp. Annu, 2006 PIREN-Seine.

Tong, Y., Xu, X., Qi, M., Sun, J., Zhang, Yiyan, Zhang, W., Wang, M., Wang, X., Zhang, Yang, 2021. Lake warming intensifies the seasonal pattern of internal nutrient cycling in the eutrophic lake and potential impacts on algal blooms. Water Res 188, 116570. https://doi.org/10.1016/j.watres.2020.116570.

Tranvik, L.J., Downing, J.A., Cotner, J.B., Loiselle, S.A., Striegl, R.G., Ballatore, T.J., Dillon, P., Finlay, K., Fortino, K., Knoll, L.B., Kortelainen, P.L., Kutser, T., Larsen, S., Laurion, I., Leech, D.M., McCallister, S.L., McKnight, D.M., Melack, J.M., Overholt, E., Porter, J.A., Prairie, Y., Renwick, W.H., Roland, F., Sherman, B.S., Schindler, D.W., Sobek, S., Tremblay, A., Vanni, M.J., Verschoor, A.M., von Wachenfeldt, E., Weyhenmeyer, G.A., 2009. Lakes and reservoirs as regulators of carbon cycling and climate. Limnol. Oceanogr. 54, 2298–2314. https://doi.org/10.4319/lo.2009.54.6_part_2.2298.

Van Cappellen, P., Maavara, T., 2016. Rivers in the Anthropocene: global scale modifications of riverine nutrient fluxes by damming. Ecohydrol. Hydrobiol. 16, 106–111. https://doi.org/10.1016/j.ecohyd.2016.04.001.

Wang, F., Maberly, S.C., Wang, B., Liang, X., 2018. Effects of dams on riverine biogeochemical cycling and ecology. Inl. Waters 8, 130–140. https://doi.org/10.1080/20442041.2018.1469335.

Wang, W.F., Li, S.L., Zhong, J., Maberly, S.C., Li, C., Wang, F.S., Xiao, H.Y., Liu, C.Q., 2020a. Climatic and anthropogenic regulation of carbon transport and transformation in a karst river-reservoir system. Sci. Total Environ. 707, 135628 https://doi.org/10.1016/j.scitotenv.2019.135628.

Wang, W., Li, S.L., Zhong, J., Wang, L., Yang, H., Xiao, H., Liu, C.Q., 2021. CO_2 emissions from karst cascade hydropower reservoirs: mechanisms and reservoir effect. Environ. Res. Lett. 16, 044013 https://doi.org/10.1088/1748-9326/ABE962.

Wang, W., Yi, Y., Zhong, J., Kumar, A., Li, S.L., 2020b. Carbon biogeochemical processes in a subtropical karst river–reservoir system. J. Hydrol. 591, 125590 https://doi.org/10.1016/j.jhydrol.2020.125590.

Weber, M., Rinke, K., Hipsey, M.R., Boehrer, B., 2017. Optimizing withdrawal from drinking water reservoirs to reduce downstream temperature pollution and reservoir hypoxia. J. Environ. Manag. 197, 96–105. https://doi.org/10.1016/J.JENVMAN.2017.03.020.

Winton, R.S., Teodoru, C.R., Calamita, E., Kleinschroth, F., Banda, K., Nyambe, I., Wehrli, B., Winton, R.S., 2021. Anthropogenic influences on Zambian water quality: hydropower and land-use change. Environ. Sci. Process. Impacts 23, 981–994. https://doi.org/10.1039/D1EM00006C.

Wu, X., Wang, Z., Xiang, X., Yang, H., Li, C., Li, S., Wu, L., 2022. Dynamic simulation of CO_2 flux in a hydropower reservoir in Southwest China. J. Hydrol. 128354 https://doi.org/10.1016/J.JHYDROL.2022.128354.

Xia, X., Liu, T., Yang, Z., Michalski, G., Liu, S., Jia, Z., Zhang, S., 2017. Enhanced nitrogen loss from rivers through coupled nitrification-denitrification caused by suspended sediment. Sci. Total Environ. 579, 47–59. https://doi.org/10.1016/j.scitotenv.2016.10.181.

Xiao, J., Wang, B., Qiu, X.L., Yang, M., Liu, C.Q., 2021. Interaction between carbon cycling and phytoplankton community succession in hydropower reservoirs: evidence from stable carbon isotope analysis. Sci. Total Environ. 774, 145141 https://doi.org/10.1016/J.SCITOTENV.2021.145141.

Xiao, W., Huang, Y., Mi, W., Wu, H., Bi, Y., 2019. Variation of diatoms and silicon in a tributary of the Three Gorges Reservoir: evidence of interaction. Water Vol. 11. https://doi.org/10.3390/W11071369, 2019Page 1369 111369.

Yan, X., Thieu, V., Garnier, J., 2021a. Long-term evolution of greenhouse gas emissions from global reservoirs. Front. Environ. Sci. 9, 289. https://doi.org/10.3389/FENVS.2021.705477/BIBTEX.

Yan, X., Thieu, V., Garnier, J., 2021b. Long-term assessment of nutrient budgets for the four reservoirs of the Seine Basin (France). Sci. Total Environ. 778, 146412 https://doi.org/10.1016/j.scitotenv.2021.146412.

Yan, X., Thieu, V., Wu, S., Garnier, J., 2022. Reservoirs change pCO_2 and water quality of downstream rivers: evidence from three reservoirs in the Seine Basin. Water Res 213, 118158. https://doi.org/10.1016/J.WATRES.2022.118158.

Zhang, Q., Blomquist, J.D., 2018. Watershed export of fine sediment, organic carbon, and chlorophyll-a to Chesapeake Bay: spatial and temporal patterns in 1984–2016. Sci. Total Environ. 619–620, 1066–1078. https://doi.org/10.1016/J.SCITOTENV.2017.10.279.